

## Research Article

# Oak tree leaves activated carbon with magnetite nanoparticles for the removal of Pb(II) ions from aqueous solutions

Walaa H. ABDULQADER\*, Jamal A. ABBAS

*Department of Chemistry, College of Science, University of Duhok, Iraq.*

*\*Email: walaa.abdulqader@uod.ac*

**Abstract:** This study aimed to produce a new adsorbent from the thick leaves that fall off Oak trees in the autumn season, which were activated by heating at several temperatures (700-900°C) after being treated with a KOH compound to obtain activated carbon (AC). It was subsequently composited with iron oxide magnetite nanoparticles (AC/Fe<sub>3</sub>O<sub>4</sub>) using the co-precipitation technique to remove Pb (II) ions from aqueous solutions in batch mode. Utilizing XRD, BET, FTIR, SEM/EDS, TEM, VSM, and TGA, the adsorbent was characterized. Variables such as contact time, PH, adsorbate concentration, temperature, and adsorbent dose were used to conduct adsorption studies of divalent lead from an aqueous solution. The optimal adsorption efficiency was found at a contact time of 60 minutes, a pH of 8, a dose of 0.4 g/L adsorbent, an initial metal ion concentration of 100mg/L, and a temperature of 25°C. The adsorption kinetic of Pb(II) onto adsorbent (AC/Fe<sub>3</sub>O<sub>4</sub> at 800°C) was discussed using different models, the pseudo-second-order model provided the best correlation of the experimental data. Langmuir, Freundlich, and Tempkin adsorption isotherms were employed in order to evaluate the optimum adsorption capacity of the adsorbent, the Freundlich model gave a better fit than Langmuir and Tempkin models. The results demonstrated that (AC/Fe<sub>3</sub>O<sub>4</sub> at 800°C) can be utilized efficiently to remove Pb(II) from polluted water.

**Keywords:** Activated carbon, Iron oxide nanoparticles, pH, TEM, XRD.

**Citation:** Abdulqader, W.H. & Abbas, J.A. 2023. Oak tree leaves activated carbon with magnetite nanoparticles for the removal of Pb(II) ions from aqueous solutions. Iranian Journal of Ichthyology (Special Issue 1): 219-237.

---

## Introduction

Water contamination with various pollutants, primarily dyes and heavy metals, is currently a major environmental issue and a threat to the health of living organisms. Heavy metals are non-biodegradable, enduring, cancer-causing, and toxic in the environment, and they are widely dispersed. Lead, copper, Cadmium, and chromium are just a few of the heavy metals found in industrial effluent (Gupta & Nayak 2012; Saleh & Gupta 2012; Sharififard et al. 2017). Lead is a pollutant that is found throughout the environment. It can be taken through food and drink that contain lead as well as through the respiration system. Due to the potential neurotoxicity of lead, it can accumulate in bone and soft tissues over time. Furthermore, it can cause a

decrease in performance (Karaca 2008).

A variety of techniques are currently available for removing heavy metals from industrial wastewater. Among them, adsorption has been demonstrated to be a well-established and low-cost pollutant removal process. Due to their unique properties, such as high-specific surface areas with porous structure, and large sorption capacities. One of the most widely used adsorbents for the filtration of both liquids and gases is activated carbon (AC) (Humphrey & Keller 1977; Ismadji et al. 2005; Spahis et al. 2008; Lin & Juang 2009). The production cost of ACs is the main drawback in their commercial use. In recent decades, research has focused on the utilization of new precursors that are inexpensive and abundant, but have high valorization potential, such as agricultural

and biomass wastes (Katsaros et al. 2007; Wibowo et al. 2007). Bean pods oil, cotton stalks, sunflower, nut shells, coal, coffee ground, bituminous, fir sawdust, and other starting materials have already been used to make AC (Wang et al. 2005; El Qada et al. 2006; Malarvizhi & Sulochana 2008; Karagöz et al. 2008; Aworn et al. 2008; Demirbas 2009; Budinova et al. 2009; Girgis et al. 2009; Deng et al. 2009; Gong et al. 2009; Rufford et al. 2009; Juan & Ke-Qiang 2009; Reffas et al. 2010).

It has been well established that agricultural waste has enormous scientific, social, and economic significance because it is widely present at no or low cost, requires simple conversion, is simple to operate, and does not require regeneration. Among agricultural waste, oak tree leaves are a promising candidate for use as a precursor in the large-scale production of AC. The oak tree is a deciduous tree that belongs to the Plantae kingdom's Fagaceae family. It is found in the Zagros Mountains and other geographical areas in the Kurdistan region of Iraq. The region is covered by a native broad-leaved forest, with oak *Quercus* accounting for roughly 90% of the total forest area (Tahir & Mezeri 2020). These plant species' leaves contain cellulose (35-50%), hemicellulose (20-35%), and lignin (15-25%). With the rest made up of ash, a tiny quantity of pectin, protein, and extractives (Muhamad et al. 2016; Kaur et al. 2018). The samples of leaves have been taken from the Zawita district the north-east of Duhok city, Kurdistan region of Iraq.

Iron oxide nanotechnology has piqued the interest of the research community in solving environmental problems (Katsaros et al. 2007). This is due to the fact that iron oxide is extremely effective at removing various types of air, water, and soil contaminants via adsorption and photo-degradation (Tran et al. 2010). Iron oxide is a premium adsorbent due to its large surface area-to-volume ratio, high biocompatibility, reusability, and low cost, excellent magnetic properties, and ease of separation using an external magnetic field (Ilankoon 2014; Dave & Chopda 2014). Despite this, one disadvantage of iron oxide is

that its particles aggregate because they have a high surface-to-volume ratio (Ojemaye et al. 2017; Ghasemi et al. 2018). In order to deal with this, surface modification is required to ensure particle stability. Coating, stabilization, and functionalization can be used to modify the surface of iron oxide nanoparticles (Sanchez et al. 2005; Lu et al. 2014).

The present study has focused on to use of AC/Fe<sub>3</sub>O<sub>4</sub> NPs to evaluate their adsorption behavior for the removal of heavy metal ions from aqueous solutions such as Pb(II). The work involves the selection of optimum conditions for maximum removal of Pb(II) such as PH, contact time, initial metal concentration, and adsorbent dosage. The application of different isotherm models is one of our objectives to determine their constant especially the maximum adsorption capacity (Q<sub>m</sub>). A kinetic study was taken into consideration it is important for determining the reaction mechanism.

### Material and methods

**Materials:** Lead nitrate Pb(NO<sub>3</sub>)<sub>2</sub> (99%), Nitric acid HNO<sub>3</sub> (99.3%), and Sodium hydroxide NaOH (98%) were supplied from Merck. FeCl<sub>3</sub>·6H<sub>2</sub>O and FeSO<sub>4</sub>·7H<sub>2</sub>O were supplied from UNI-CHEM chemical reagents. KOH was supplied by POCH SA. A stock solution of Pb(II) 1000mg/L was prepared by dissolving Pb(NO<sub>3</sub>)<sub>2</sub> in deionized water. This solution was used for further experimental solution preparation. The pH values were adjusted with HNO<sub>3</sub> or NaOH. Using a pH meter calibrated with buffers solution of pH 4.0, 7.0, and 10.0. The Pb(II) content in the adsorption solutions was determined by Atomic Absorption spectrometry (AAS).

**Synthesis of activated carbon and nanoparticles:** Oak tree leaves, used to make the precursor for the activated carbon, were washed with deionized water to eliminate any dust or grime, and dried in an electro-thermostatic oven at 100°C, then it was burned in the furnace at 400°C for 1h. The resulting slurry was taken out of the furnace and washed sequentially with 0.1mol/L HCl and deionized water once it had cooled down then crushed and put

through a 63 $\mu$ m sieve after being ground into a fine powder.

To obtain chemical activation using alkali hydroxide such as KOH, Oak leaves were treated with KOH compound at a 1:1 impregnation ratio (defined as a mass ratio of KOH: precursor) for 1.5 hours, then carbon powders were thermally activated in a muffle furnace for one hour at temperatures ranging from 700-900°C. After being taken out of the oven, the resulting slurry was washed with 0.1mol/L HCl, then hot water, and finally, cold deionized water to neutralize the pH. After being filtered, they were dried in a 100°C oven for 24 hours before being used (Li et al. 2020). The nanocomposite (AC/Fe<sub>3</sub>O<sub>4</sub>) was synthesized using a modified version of the method described in Jain et al. (2018).

Activated carbon was combined with magnetite nanoparticles to create the composite (AC/MNPs) by using FeCl<sub>3</sub>.6H<sub>2</sub>O, FeSO<sub>4</sub>.7H<sub>2</sub>O and a solution of KOH. The following solutions were prepared: 10g salt/100ml DW, from both FeCl<sub>3</sub>.6H<sub>2</sub>O and FeSO<sub>4</sub>.7H<sub>2</sub>O. A 16ml solution of FeCl<sub>3</sub>.6H<sub>2</sub>O and 8ml solution of FeSO<sub>4</sub>.7H<sub>2</sub>O were thoroughly mixed with 1.0g of activated carbon for 10 minutes. Under a mechanical stirrer at 80°C, the resulting mixture was titrated against a 0.15M KOH solution until the pH was increased to 10-11, precipitating the hydrated iron oxide. Extra time was spent stirring the suspension at 80°C. After that, it remained at room temperature for one day. Magnets were used to separate the AC/Fe<sub>3</sub>O<sub>4</sub> nanocomposites, which were then washed in ethanol and distilled water until the pH was neutral. They were subsequently dried for 12 hours at 80°C in a vacuum drying oven. The AC/MNPs were then ground up and placed in sealed glass containers to be used later.

**Characterization:** Several techniques were employed to evaluate the characteristics of AC, Fe<sub>3</sub>O<sub>4</sub>, and AC/Fe<sub>3</sub>O<sub>4</sub> and to investigate their adsorption mechanisms. With the use of Field Emission Scanning Electron Microscopy (FESEM), the surface morphology of the Fe<sub>3</sub>O<sub>4</sub> and AC/Fe<sub>3</sub>O<sub>4</sub> particles was discovered (TESCAN, MIRA III, Czech). As a

technique for determining the particles' chemical composition, EDS was attached to a FESEM. In this way, EDS spectroscopy was used to determine the elemental composition of Fe<sub>3</sub>O<sub>4</sub> and AC/Fe<sub>3</sub>O<sub>4</sub>.

TGA (TA, Q600, USA) was used to study the thermal stability of materials. Surface areas were calculated using BET (BEL, BELSORP MINI II, Japan) and nanoparticles' magnetic characteristics were examined with a Vibrating Sample Magnetometer (WEISTRON, VSM1100, Taiwan). The FT-IR spectra of AC, Fe<sub>3</sub>O<sub>4</sub>, AC/Fe<sub>3</sub>O<sub>4</sub>, and metal-loaded AC/Fe<sub>3</sub>O<sub>4</sub> were obtained in the wavenumber range of 400-4000cm<sup>-1</sup> using an FT-IR spectrometer (SHIMADZU, 1800, Japan).

An analytical X'Pert high-score (Philips, PW1730, Hollanda) X-ray diffractometer with Cu-K $\alpha$ 1 radiations estimated the crystalline size of the adsorbents ( $\lambda = 1.540598 \text{ \AA}$ ),  $k$  is known as the Scherer's constant (0.94),  $\beta$  (full width at half maximum of the peak), and  $\theta$  (diffraction angle) at 40 kV and 30mA. A  $2\theta$  range was obtained from 10 to 80. The Debye-Scherrer formula:  $D = (k\lambda/\beta \cos \theta)$  was used to calculate the crystallite size ( $D$ ) (Iqbal et al. 2019). Electrolyte solutions were used to determine the pH-Point Zero Charge (PHpzc) of AC/Fe<sub>3</sub>O<sub>4</sub> NPs. The PHpzc was determined by using an aqueous solution containing 0.01M NaCl. With 0.1M HCl and 0.1M NaOH, the initial pH of the solution was adjusted to a range of 2-12; 50mL of this solution was then added to conical flasks containing 0.15g of AC/Fe<sub>3</sub>O<sub>4</sub> NPs. After 24 hours of shaking in a shaker water bath, the final pH of the solution was measured with a pH meter. The value of PHpzc was determined by graphing the relationship between pH final and pH initial. The PHpzc of the nanoparticles was determined by finding the point of intersection between the final and initial pH values (Jain et al. 2018; Imran et al. 2019, 2020).

#### **Batch adsorption studies**

**Effect of pH on adsorption:** Adsorption experiments were carried out in a solution of pH 3, 5, 6, 8, 10 and 12. The effect of initial pH on the Lead ions adsorption onto the adsorbent was determined (Table

**Table 1.** Effect of pH on adsorption of Pb(II) ions, 50mg/L solution, onto (AC/Fe<sub>3</sub>O<sub>4</sub> NPs, 800°C) 0.4g/L, at 25°C and agitation speed 150 rpm for 60 minutes.

PH	C <sub>e</sub> mg/L	q <sub>e</sub> mg/g	R%
3	22.84	67.900	54.32
5	18.7	78.25	62.6
6	11.45	96.375	77.1
8	0.31	124.225	99.38
10	1.86	120.350	96.28
12	5.708	110.75	88.6

**Table 2.** Effect of initial concentration on adsorption of Pb(II) ions onto (AC/Fe<sub>3</sub>O<sub>4</sub> NPs, 700°C) 0.4g/L was used, at pH 8 for 60 minutes, at 25°C and agitation speed 150rpm.

C <sub>i</sub> mg/L	C <sub>e</sub> mg/L	q <sub>e</sub> mg/g	R%
50	0.345	124.145	99.316
75	6.451	171.3725	91.398
100	13.859	215.3525	86.141
125	28.074	242.315	77.541
150	36.810	282.975	75.46

**Table 3.** Effect of initial concentration on adsorption of Pb(II) ions onto (AC/Fe<sub>3</sub>O<sub>4</sub> NPs, 800°C) 0.4g/L was used, at pH 8 for 60 minutes, at 25°C and agitation speed 15rpm.

C <sub>i</sub> mg/L	C <sub>e</sub> mg/L	q <sub>e</sub> mg/g	R%
50	0.281	124.297	99.438
75	5.869	172.827	92.174
100	12.177	219.557	87.823
125	26.849	245.377	78.521
150	35.948	285.13	76.0346

1). In all batch experiments, samples were collected from duplicate flasks filtered by qualitative filter paper 102 moderate, and the filtrate was analyzed for residual Lead concentration. The amount of Pb(II) adsorbed onto adsorbent, q<sub>e</sub> mg/g, was calculated using the following equation:

$$q_e = \frac{(C_i - C_e) \times V}{m}$$

Where: C<sub>i</sub> and C<sub>e</sub> are the initial and equilibrium liquid-phase concentration (mg/L) of Pb(II) respectively, V is the volume of the solution (L) and m is the weight of the adsorbent used (g). The Pb(II) percent removal R% was calculated using the following equation:

$$R\% = \frac{(C_i - C_e)}{C_i} \times 100$$

**Effect of initial concentration of pb(II) ions:** The

adsorption rate was calculated by performing experiments with varying initial lead ion concentrations, from 50-150mg/L. The remaining variables were held constant (Tables 2, 3 and 4).

**Effect of contact time:** Kinetic studies were done at pH 8 solution by shaking 0.4g/L of the activated carbon (AC/Fe<sub>3</sub>O<sub>4</sub> NPs, 800°C) in 25ml of lead nitrate solution 100mg/L at 25°C. The batch experiments were carried out at different time intervals. The data of lead ions adsorption were stated in Table 5.

**Effect of dose:** The effect of sorbent dose on the removal of 100mg/L pb(II) was studied using different doses of (AC/Fe<sub>3</sub>O<sub>4</sub> NPs, 800°C), at 25°C, pH 8 for 1 h, and agitation speed 150rpm (Table 6).

**Adsorption isotherm:** Adsorption isotherm experiments were carried out at different temperatures and varying initial concentrations of

**Table 4.** Effect of initial concentration on adsorption of Pb(II) ions onto activated carbon (AC/Fe<sub>3</sub>O<sub>4</sub> NPs, 900°C) 0.4g/L was used, at pH 8 for 60 minutes, at 25°C and agitation speed 150rpm.

C <sub>i</sub> mg/L	C <sub>e</sub> mg/L	q <sub>e</sub> mg/g	R%
50	0.581	123.547	98.838
75	7.529	168.677	89.961
100	15.871	210.3225	84.129
125	30.213	236.9675	75.829
150	39.095	277.2625	73.9366

**Table 5.** Effect of contact time on the adsorption of Pb(II), 100mg/L solution, onto activated carbon (AC/Fe<sub>3</sub>O<sub>4</sub> NPs, 800°C), 0.4g/L, at 25°C, pH 8, and agitation speed 150rpm.

Time (min)	C <sub>e</sub> mg/L	q <sub>t</sub> mg/g	q <sub>e</sub> -q <sub>t</sub> mg/g	log(q <sub>e</sub> -q <sub>t</sub> ) mg/g	t/q <sub>t</sub> min.g.mg <sup>-1</sup>	ln t min	t <sup>1/2</sup> min <sup>1/2</sup>	R%
10	15.36	211.6	17.5	1.24304	0.04725	2.3025	3.1623	84.64
20	15	212.5	16.6	1.22011	0.09412	2.9957	4.4721	85
40	13.85	215.36	13.73	1.13775	0.18573	3.6888	6.3246	86.147
60	12.54	218.64	10.46	1.01943	0.27442	4.0943	7.7459	87.457
80	11.335	221.66	7.438	0.87143	0.36091	4.3820	8.9443	88.665
100	9.73	225.67	3.425	0.53466	0.44312	4.6052	10	90.27
120	8.5	228.75	0.35	-0.45593	0.52459	4.7875	10.954	91.5
140	8.36	229.1	0		0.61109	4.9416	11.832	91.64

**Table 6.** The effect of sorbent dose on the removal of 100mg/L pb(II) was studied using different dose of (AC/Fe<sub>3</sub>O<sub>4</sub> NPs, 800°C), at 25°C, pH 8, for 1 h, and agitation speed 150rpm.

AC/Fe <sub>3</sub> O <sub>4</sub> NPs, conc. (g/L)	C <sub>e</sub> mg/L	q <sub>e</sub> mg/g	R%
0.2	20.372	398.14	79.628
0.4	12.607	218.48	87.393
1.2	8.393	76.339	91.607
2	5.630	47.185	94.37
3.2	1.091	30.909	98.909

Pb(II), while the adsorbent dosage and pH were held constant. All isotherm experiments were done using a linear thermostat shaker (Table 7).

## Results and Discussion

**Characterization:** A powder X-ray diffractometer was used to collect the diffraction data for the Fe<sub>3</sub>O<sub>4</sub> and AC/Fe<sub>3</sub>O<sub>4</sub> samples under inspection. Data were collected using a continuous scanning mode and a position-sensitive X'Celerator detector with a step size of 0.05° and a range of 10.24 to 70.99°. Scherrer equation was applied to determine the average grain size of magnetic nanoparticles: Scherrer Formula:

$D_p = (K \lambda) / (\beta \cos \theta)$ , where,  $D_p$  is the average grain size,  $k$  is the shape-dependent Scherrer's constant (0.90), and  $\lambda$  is the X-ray wavelength (1.5406 Å),  $\beta$  = full width at half maximum intensity (FWHM given in radians), and  $\theta$  is (diffraction angle) at 40kV and 30mA.

Analysis of crystal size using the Scherrer equation revealed that the crystal size of both magnetite nanoparticles (~ 4 to 18nm) is almost similar (Fig. 1). Figure 2 displays SEM micrographs of Fe<sub>3</sub>O<sub>4</sub>, AC/Fe<sub>3</sub>O<sub>4</sub>. SEM images provide an overview of the structure and form of the examined nanoparticles. Fe<sub>3</sub>O<sub>4</sub> and AC/Fe<sub>3</sub>O<sub>4</sub> in Figure 2 (a

**Table 7.** Equilibrium parameters for the adsorption of pb(II) ions, onto (AC/Fe<sub>3</sub>O<sub>4</sub> NPs, 800°C), 0.4 mg/L, PH8, for 60 minutes and agitation speed 150 rpm. (At 25°C= 298 K)

C <sub>i</sub> mg/L	C <sub>e</sub> mg/L	q <sub>e</sub> mg/g	log q <sub>e</sub> mg/g	logC <sub>e</sub> mg/L	lnC <sub>e</sub> mg/L	1/ q <sub>e</sub> g mg <sup>-1</sup>	1/C <sub>e</sub> L mg <sup>-1</sup>
75	5.869	172.827	2.2376	0.7685	1.7697	0.00578	0.1703
100	12.177	219.557	2.3415	1.0855	2.4995	0.00455	0.082
125	26.849	245.377	2.3898	1.4289	3.2902	0.00407	0.037
150	35.948	285.13	2.4550	1.5556	3.5821	0.00351	0.0278
At 35°C = 308 K							
C <sub>i</sub> mg/L	C <sub>e</sub> mg/L	q <sub>e</sub> mg/g	log q <sub>e</sub> mg/g	logC <sub>e</sub> mg/L	lnC <sub>e</sub> mg/L	1/ q <sub>e</sub> g mg <sup>-1</sup>	1/C <sub>e</sub> L mg <sup>-1</sup>
75	4.147	177.1325	2.2483	0.6177	1.4224	0.00564	0.2411
100	10.335	224.1625	2.3505	1.0143	2.3355	0.00446	0.0967
125	22.617	255.9575	2.4081	1.3544	3.1187	0.00391	0.0442
150	33.130	292.175	2.4656	1.5202	3.5004	0.00342	0.0302
At 45°C= 318 K							
C <sub>i</sub> mg/L	C <sub>e</sub> mg/L	q <sub>e</sub> mg/g	log q <sub>e</sub> mg/g	logC <sub>e</sub> mg/L	lnC <sub>e</sub> mg/L	1/ q <sub>e</sub> g mg <sup>-1</sup>	1/C <sub>e</sub> L mg <sup>-1</sup>
75	2.682	180.795	2.2572	0.4284	0.9865	0.00553	0.3728
100	7.056	232.36	2.3662	0.8485	1.9538	0.00430	0.1417
125	20.261	261.84	2.4180	1.3066	3.0087	0.00382	0.0493
150	31.691	295.772	2.4709	1.5009	3.4560	0.00338	0.0315
At 55°C= 328 K							
C <sub>i</sub> mg/L	C <sub>e</sub> mg/L	q <sub>e</sub> mg/g	log q <sub>e</sub> mg/g	logC <sub>e</sub> mg/L	lnC <sub>e</sub> mg/L	1/ q <sub>e</sub> g mg <sup>-1</sup>	1/C <sub>e</sub> L mg <sup>-1</sup>
75	0.873	185.3175	2.2679	-0.0589	-0.1358	0.00539	1.1454
100	4.427	238.9325	2.3783	0.6461	1.4877	0.00418	0.2258
125	17.126	269.685	2.4308	1.2336	2.8406	0.00371	0.0584
150	28.481	303.7975	2.4826	1.4545	3.3492	0.00329	0.0351

and b) show that the nanoparticles are clumped together and adhered to one another, resulting in a rough and coarse surface. The weight fraction of iron in the EDS spectra of the Fe<sub>3</sub>O<sub>4</sub> nanoparticles sample (Fig. 3), is 63.9% and it does not contain carbon, in contrast, the weight fraction of iron content in the AC/Fe<sub>3</sub>O<sub>4</sub> (Fig. 3), is only 16.1% while the carbon is 59.5% that's confirmed by the sharp peaks of carbon and iron, indicated that the percentage of activated carbon was much higher than that of Fe<sub>3</sub>O<sub>4</sub> NPs.

The TEM images and particle size distribution of the synthesized Fe<sub>3</sub>O<sub>4</sub> and AC/Fe<sub>3</sub>O<sub>4</sub> nanoparticles are given in Figures 4a, b, c, and d. The co-

precipitation method produces nanoparticles with average particle sizes of 27nm for Fe<sub>3</sub>O<sub>4</sub> and 17nm for AC/Fe<sub>3</sub>O<sub>4</sub>, and this could be attributed to the aggregation of iron oxide nanoparticles. TGA/DTG curves in Argon atmosphere at a heating rate of 20°C min<sup>-1</sup> were used to measure variations in the mass of Fe<sub>3</sub>O<sub>4</sub> and AC/Fe<sub>3</sub>O<sub>4</sub> as a function of temperature in a defined and controlled environment from 20 to 810°C. The thermal stabilities of Fe<sub>3</sub>O<sub>4</sub> and AC/Fe<sub>3</sub>O<sub>4</sub> were evaluated using TGA, with the weight change during heating in an Argon atmosphere used as an indicator of thermal stability. Figure 5 depicts the mass loss (TGA) curves of Fe<sub>3</sub>O<sub>4</sub>

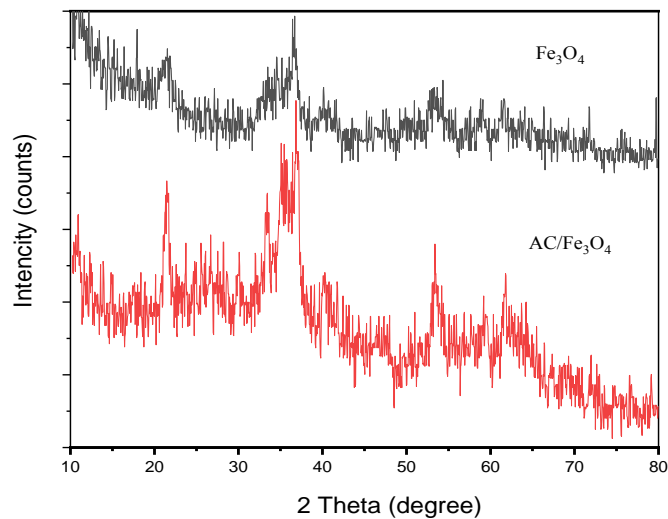


**Fig.1.** XRD distribution of  $\text{Fe}_3\text{O}_4$  and  $\text{AC}/\text{Fe}_3\text{O}_4$ .

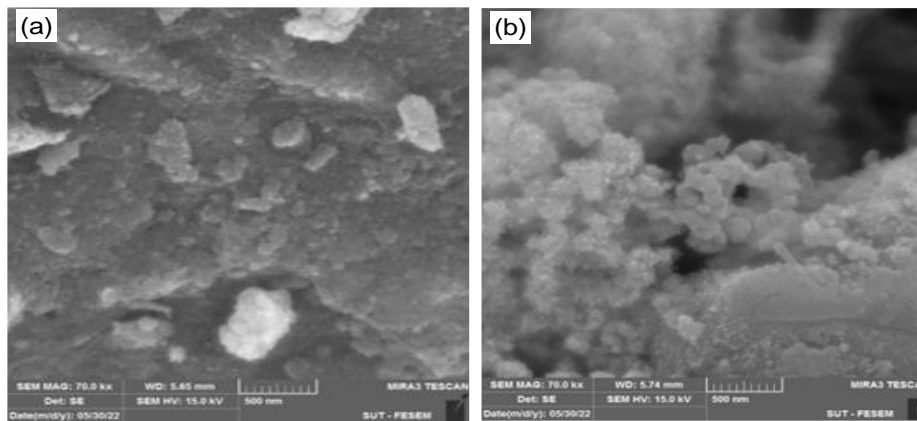


**Fig.2.** SEM image of: a)  $\text{Fe}_3\text{O}_4$  and b)  $\text{AC}/\text{Fe}_3\text{O}_4$ .

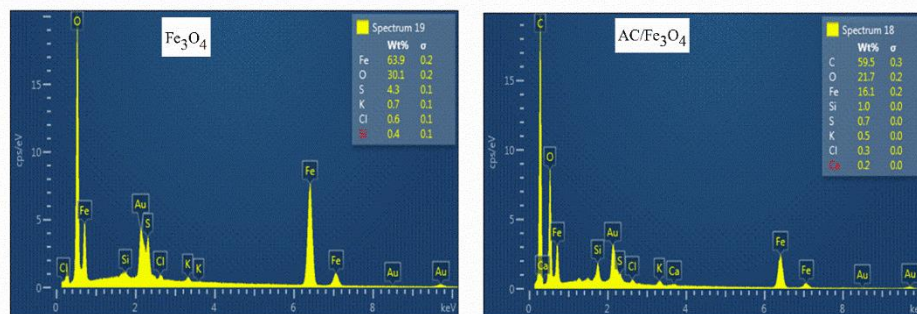


**Fig.3.** EDS spectra of  $\text{Fe}_3\text{O}_4$  and  $\text{AC}/\text{Fe}_3\text{O}_4$ .

and  $\text{AC}/\text{Fe}_3\text{O}_4$ . The TGA peaks indicate that  $\text{Fe}_3\text{O}_4$  degraded in two steps (Fig. 5). The maximum weight loss (14.89%) was observed at the first peak, which was around  $215^\circ\text{C}$ , and was attributed to the loss of moisture and other compounds, that most likely came from the raw material. The removal of chemically bound moisture was represented by the second peak at  $259^\circ\text{C}$  in the temperature range from 215 to  $800^\circ\text{C}$ ,

with an additional 11.48 percent weight loss. As a result, iron oxide was the sole residue at the end of the degradation, with a residual mass of 73.62%. In contrast, the degradation of  $\text{AC}/\text{Fe}_3\text{O}_4$  occurred in three distinct stages, as indicated by the TGA peaks. The initial weight loss (below  $110^\circ\text{C}$ ) was 4.02% caused primarily by moisture loss. A second peak at around  $405^\circ\text{C}$  with a high weight loss of 42.77% was

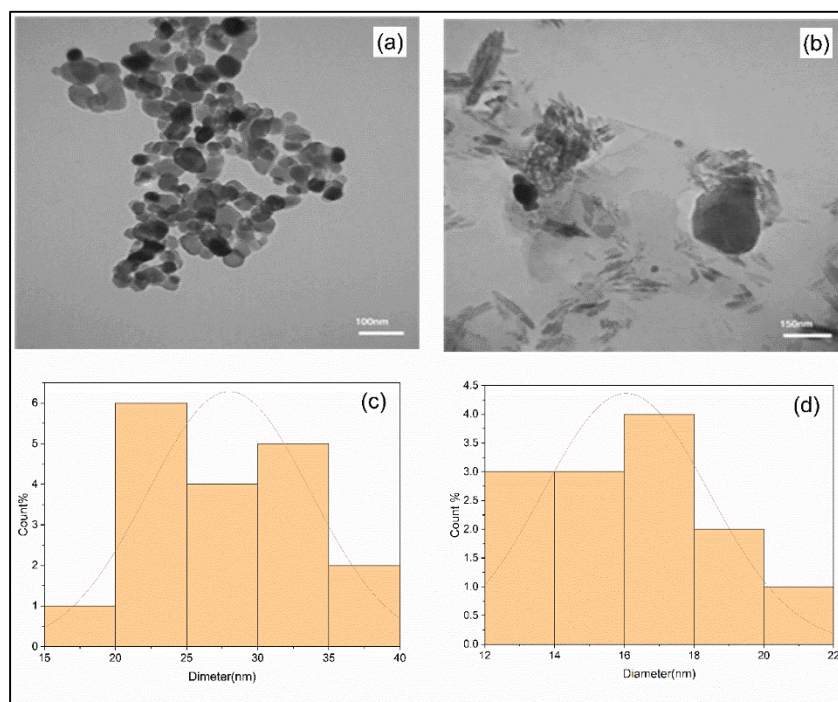


**Fig.4.** TEM images of **a)**  $\text{Fe}_3\text{O}_4$ , **b)**  $\text{AC}/\text{Fe}_3\text{O}_4$ , **c)** Particle size distribution of  $\text{Fe}_3\text{O}_4$ , **d)** Particle size distribution of  $\text{AC}/\text{Fe}_3\text{O}_4$  and in the inset, selected area diffraction pattern of  $\text{Fe}_3\text{O}_4$  and  $\text{AC}/\text{Fe}_3\text{O}_4$ .

**Table 8.** Show the yields and pore structural parameters of activated carbons and  $\text{AC}/\text{Fe}_3\text{O}_4$  nanoparticles upon carbonation.

Sample	Surface $\text{BET}$ $\text{m}^2/\text{g}$	micropore surface area ( $S_{\text{mic}}$ ) $\text{m}^2/\text{g}$	external surface area ( $S_{\text{ext}}$ ) $\text{m}^2/\text{g}$	Total Volume ( $V_{\text{tot}}$ ) $\text{cm}^3/\text{g}$	Micropor e volume ( $V_{\text{mic}}$ ), $\text{cm}^3/\text{g}$	Percentage of micro-pore	Average pore diameter $D_p$ nm
AC	630.2	54.5	575.7	0.3495	0.0582	16.6	2.21
$\text{AC}/\text{Fe}_3\text{O}_4$	397.88	112.55	285.33	0.2776	0.1478	53	2.79

$D_p$  was calculated as;  $D_p = 4V_{\text{Tot}}/\text{SBET}$  ( $\text{SBET} = \text{mean} \pm \text{standard deviation}$ ).

observed due to the thermal degradation of cellulose and hemicellulose (Yao et al. 2016). The third stage ranged from  $516^\circ\text{C}$ , with the slow weight loss caused by lignin pyrolysis in biomass (Ferdous et al. 2002; Wang et al. 2008). More than  $800^\circ\text{C}$ , a final residual mass of 37.33% was identified, which could be representative of materials including iron oxide and other carbonaceous residuals.

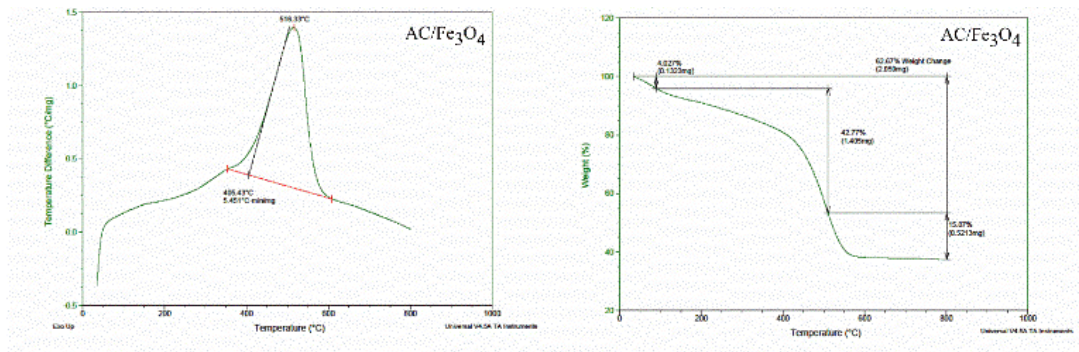
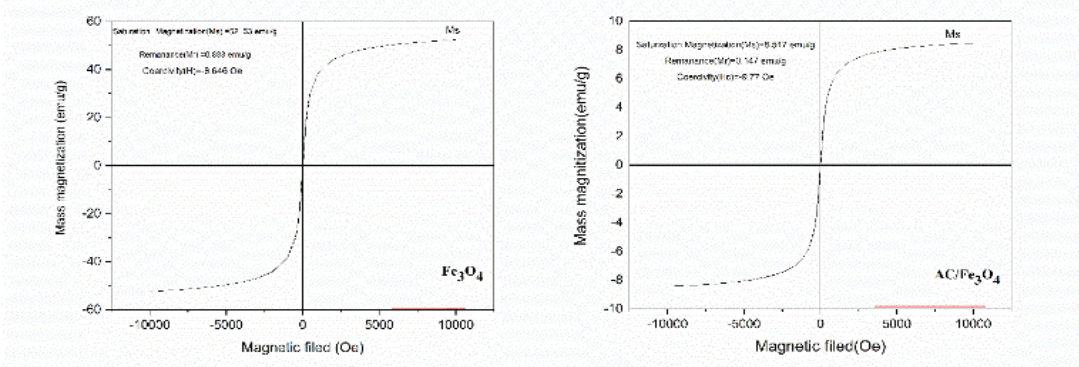
The surface properties of activated carbon were determined using an automatic surface area and porosity analyzer and  $\text{N}_2$  adsorption at (77K). The total pore volume of  $\text{AC}/\text{Fe}_3\text{O}_4$  was  $0.2776\text{cm}^3/\text{g}$ , and the average pore diameter was greater than 2nm, indicating that the carbons were highly mesoporous (Table 8). The BET had a total surface area of

$397.88\text{m}^2/\text{g}$ .

The magnetic hysteresis loop (Fig.6) of iron oxide nanoparticles was plotted against the magnetic field and mass magnetization ratio (M).  $M_s$ , which measures maximum magnetic strength, was measured to be 52.53 and  $8.517\text{emu/g}$  for  $\text{Fe}_3\text{O}_4$  and  $\text{AC}/\text{Fe}_3\text{O}_4$ , respectively. Both nanoparticles have lower  $M_s$  values than pure magnetite ( $\text{Fe}_3\text{O}_4$ ), which has a value of  $92\text{emu/g}$  (Dunlop & Özdemir 2001). This decline in magnetization, however, had no influence on the attraction by the external magnet, as  $\text{AC}/\text{Fe}_3\text{O}_4$  was still strongly attracted by the external magnet.  $\text{Fe}_3\text{O}_4$  and  $\text{AC}/\text{Fe}_3\text{O}_4$  coercivities ( $H_c$ ) are -8.646 and  $-9.770\text{Oe}$ , respectively, indicating that the nanoparticles are ferromagnetic. For  $\text{Fe}_3\text{O}_4$  and

**Table 9.** Shows the magnetic properties of Fe<sub>3</sub>O<sub>4</sub> and AC/Fe<sub>3</sub>O<sub>4</sub>.

Nanoparticles	Saturation magnetization (emu/g)	Remanent magnetization (emu/g)	Coercivity (Oe)
Fe <sub>3</sub> O <sub>4</sub>	52.53	0.888	-8.646
AC/Fe <sub>3</sub> O <sub>4</sub>	8.517	0.147	-9.77

**Fig.5.** TGA/DTG profile of Fe<sub>3</sub>O<sub>4</sub> and Fe<sub>3</sub>O<sub>4</sub>/AC.**Fig.6.** Magnetic moment loop of Fe<sub>3</sub>O<sub>4</sub> and AC/Fe<sub>3</sub>O<sub>4</sub>.

AC/Fe<sub>3</sub>O<sub>4</sub>, the remnant magnetization (Mr) is 0.888 and 0.147 (emu/g), respectively (Table 9). As a result, Fe<sub>3</sub>O<sub>4</sub> and AC/Fe<sub>3</sub>O<sub>4</sub> with these saturation magnetization values can respond to an external magnetic field, causing heavy metal separation from an aqueous solution.

The FT-IR spectra of AC, Fe<sub>3</sub>O<sub>4</sub>, AC/Fe<sub>3</sub>O<sub>4</sub>, and metal-loaded AC/ Fe<sub>3</sub>O<sub>4</sub> show the functional groups and their corresponding frequencies (Fig. 7). The wide transmission band was responsible for the continuous stretching and vibration of O-H (phenolic and alcoholic) at 3645-3703cm<sup>-1</sup> and 3410cm<sup>-1</sup> for AC and AC/Fe<sub>3</sub>O<sub>4</sub> respectively. In the absorption band peak at wave number 2357cm<sup>-1</sup> AC and 2195cm<sup>-1</sup> AC/Fe<sub>3</sub>O<sub>4</sub>, these vibrations are caused by the C=O group. Transmission 14588 cm<sup>-1</sup> for AC and

1527cm<sup>-1</sup> AC/Fe<sub>3</sub>O<sub>4</sub> showed C=C stretching vibration mode and the transmission at 1600 cm<sup>-1</sup> for AC and 1597cm<sup>-1</sup> for AC/Fe<sub>3</sub>O<sub>4</sub> was attributed to the aldehyde group with C-H stretching vibration. While transmission at 875cm<sup>-1</sup> for AC and 713cm<sup>-1</sup> for AC/Fe<sub>3</sub>O<sub>4</sub> was attributed to ether (-C-O) vibration stretching, weak transmission at 1026cm<sup>-1</sup> and 1130cm<sup>-1</sup> indicates C-H (Rocking) for AC and AC/Fe<sub>3</sub>O<sub>4</sub> respectively. Wave numbers at 416-594cm<sup>-1</sup> for AC and 424-447cm<sup>-1</sup> for AC/Fe<sub>3</sub>O<sub>4</sub> attribute to the CH group of aromatics respectively.

In accordance with the characteristic stretching band of Fe-O on Fe<sub>3</sub>O<sub>4</sub>, AC/Fe<sub>3</sub>O<sub>4</sub>, and Pb loaded on AC/Fe<sub>3</sub>O<sub>4</sub>, the bands 613.36, 628.79, and 6609cm<sup>-1</sup> indicate the formation of magnetic nanoparticles. There was a variation in the transmission and shift in

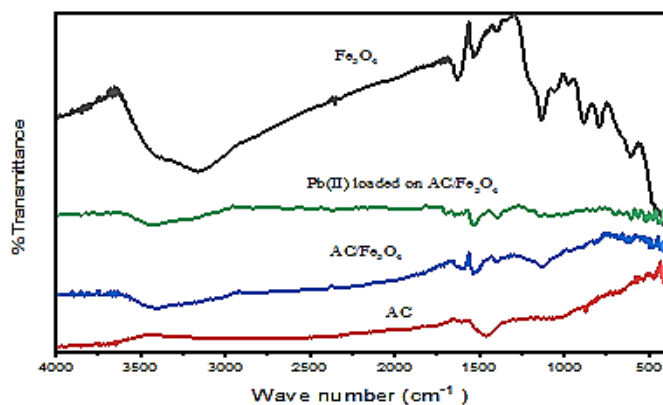


**Fig.7.** FTIR spectra of  $\text{Fe}_3\text{O}_4$ , Pb (II) loaded AC/  $\text{Fe}_3\text{O}_4$ , AC/  $\text{Fe}_3\text{O}_4$  and AC.

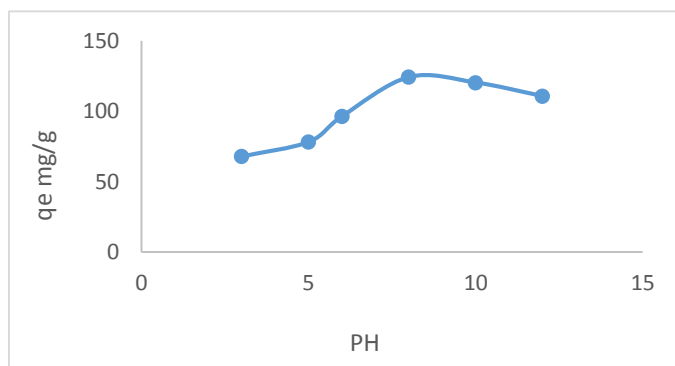


**Fig.8.** Effect of pH on adsorption of Pb(II) ions, 50mg/L solution, onto adsorbent (AC/ $\text{Fe}_3\text{O}_4$  NPs, 800°C) 0.4g/L,  $q_e$ .

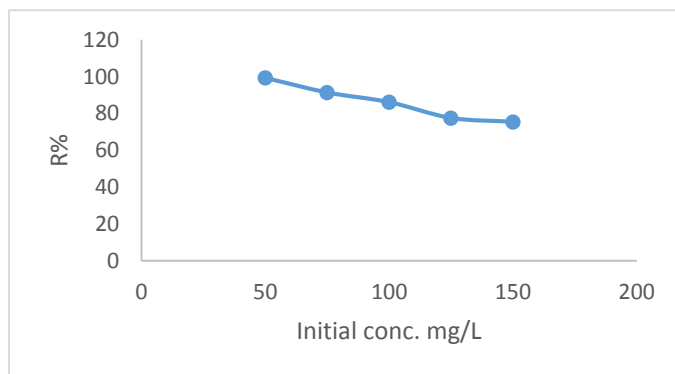


**Fig.9.** Relation between amount of Pb(II) adsorbed at equilibrium, using (AC/ $\text{Fe}_3\text{O}_4$  NPs, 800°C) 0.4g/L at pH 8, time 60 min., temperature 25°C, R% vs. initial conc.

the position of peak transmission after the attachment of Pb on the surface of AC/ $\text{Fe}_3\text{O}_4$ . These changes in FTIR spectra confirm the complexation of Pb(II) with functional groups present on the nanoparticles (Jain et al. 2018; Li et al. 2020; Rampe et al. 2021).

**Effect of pH on the Pb(II) adsorption:** pH is a significant factor in heavy metal adsorption from aqueous solutions. Table 1 and Figure 8 show the effect of the solution pH on the adsorption of Pb(II) ions, 50mg/L solution, onto (AC/ $\text{Fe}_3\text{O}_4$  NPs at

800°C) 0.4g/L. The measurement of the point zero charges (PZC) of adsorbents is essential for determining their pH-dependent behavior. It illustrates the pH value at which the net charge on the surface of particles becomes zero under varied parameters of applied pressure, the composition of the aqueous solution, and temperature (Bakatula et al. 2018). The findings of this research revealed that the PZC for AC/ $\text{Fe}_3\text{O}_4$  NPs was pH 7.8. For heavy metal immobility, the electrostatic interaction between

nanoparticles and metal ions is essential. The  $Pb^{2+}$  ions are bound to the nanoparticles' positively charged surface through electrostatic interaction when the solution's pH is below that of the PZC. Above  $pH_{PZC}$  7.8, where the surface charge of the nanoparticles was negative, an electrostatic attraction developed between the nanoparticles' surface and  $Pb(II)$  ions (Imran et al. 2020).

**Effect of initial concentration:** The initial concentration of lead ions ( $Pb(II)$ ) in aqueous solutions has a significant influence on the amount of lead that can be adsorbed. In this work, the initial concentration of  $Pb(II)$  is changed from 50 to 150mg/L, keeping the adsorbent dosage at 0.4g/L. Figure 9 and Table 3 illustrate the influence of initial concentration on the percentage of  $Pb(II)$  ions removed. The removal percentage decreased from 99.43% (at  $Pb(II)$  conc.50mg/L) to 76.03% (at  $Pb(II)$  conc.150mg/L) using the same adsorption temperature and contact time. There may be a correlation between the concentration of metal ions and the decrease in removal efficiency; this correlation may be explained by the fact that as the concentration of metal ions rises, a greater percentage of surface sites are occupied, due to a lack of available free binding sites, the adsorption capacity of the nanoparticles is reduced, leading to a drop in removal effectiveness. Since there are more active sites on the surface of the adsorbent at low concentrations, it follows that the percentage of adsorption is also high at these concentrations (Jain et al. 2018).

**Effect of contact time:** The maximum  $Pb(II)$  adsorption capacity was determined by observing the impact of contact time (Adebayo 2013). At a fixed initial  $Pb(II)$  concentration of 100mg/L, the contact time ranged from 10 to 140 minutes. Figure 10 demonstrates a gradual increase in the rate of percent lead removal. This is probably due to the surface area of the activated carbon being available at the beginning of the adsorption of  $Pb(II)$  ions (Saeed et al. 2005). The uptake rate is controlled by the rate at which the adsorbate is transported from the exterior

to the interior sites of the adsorbent particles (Malik 2003; Mall et al. 2005). A contact time of 60 minutes was considered to be the optimum and most economical time for subsequent experiments.

**Effect of dose:** Removal effectiveness is significantly affected by the adsorbent dose. The use of the optimal dose in the process of contaminant removal is essential and efficient in terms of cost. Dosage effects on  $Pb(II)$  removal by (AC/ $Fe_3O_4$  NPs, 800°C) are shown in Figure 11 and Table 6 for doses ranging from 0.2 to 3.2g/L, maintained at pH 8, and 100mg/L of  $Pb(II)$ .  $Pb$  removal from polluted water was shown to be proportional to the amount of adsorbent used. The maximum  $Pb$  removal by AC/ $Fe_3O_4$  NPs, 800°C at 3.2g/L was 98.9. While it was 79.6 at a dose of 0.2g/L. With higher doses of activated carbon, adsorption efficiency is reduced. This decreased  $Pb$  adsorption was attributed to aggregates forming at high adsorbent dosages or to the partial use of active sites (Imran et al. 2020).

**Adsorption isotherm:** The adsorption isotherm, which is composed of constant values that describe the surface properties and affinity of the adsorbent, can be used to figure out how much an adsorbent can hold. The equilibrium data were analyzed using different isotherm models in order to select one that could be employed in the design process (El Nemr 2007). Langmuir, Freundlich, and Tempkin are the models used to investigate the adsorption of lead ions via(AC/ $Fe_3O_4$  NPs at 800°C. In general, the correlation coefficients indicate that isotherm equations are applicable.

**Langmuir isotherm equation:** The experimental data are analyzed according to the liner form of Langmuir isotherm represented by the following equation (Vazquez et al. 2002).

$$\frac{1}{q_e} = \left(\frac{1}{K_L Q_m}\right) \frac{1}{C_e} + \frac{1}{Q_m}$$

Where  $C_e$  is the equilibrium concentration mg/L,  $q_e$  is the amount adsorbed at equilibrium (mg/g) and  $Q_m$  is the maximum Langmuir adsorption capacity

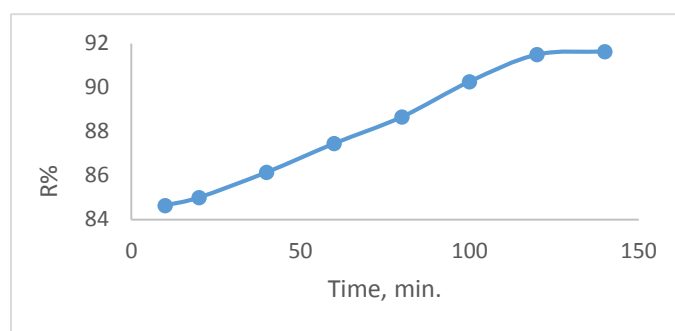


**Fig.10.** Effect of contact time on Pb(II) removal using (AC/Fe<sub>3</sub>O<sub>4</sub> NPs, 800°C) 0.4g/L, at pH 8, temp. 25°C, R% vs. Time.

**Table 10.** Comparison of the coefficients isotherm parameters from lead adsorption onto (AC/Fe<sub>3</sub>O<sub>4</sub> NPs, 800°C).

Isotherm model	Isotherm parameter	Temperature °C			
		25	35	45	55
Langmuir	Q <sub>m</sub> (mg/ g)	303.03	294.117	294.117	285.714
	K <sub>L</sub> (L mg <sup>-1</sup> )	0.226	0.3505	0.5862	2.0588
	R <sup>2</sup>	0.9657	0.9647	0.9744	0.9299
Freundlich	K <sub>F</sub>	112.098	128.233	153.78	190.502
	n	3.9478	4.3308	5.34188	7.44047
	R <sup>2</sup>	0.9629	0.9893	0.9717	0.9833
Tempkin	A <sub>T</sub>	3.71969	6.80879	25.1979	379.302
	B <sub>T</sub>	56.287	52.601	43.508	31.881
	b <sub>T</sub>	44.0167	48.6818	60.767	85.5365
	R <sup>2</sup>	0.9541	0.9813	0.9762	0.9778

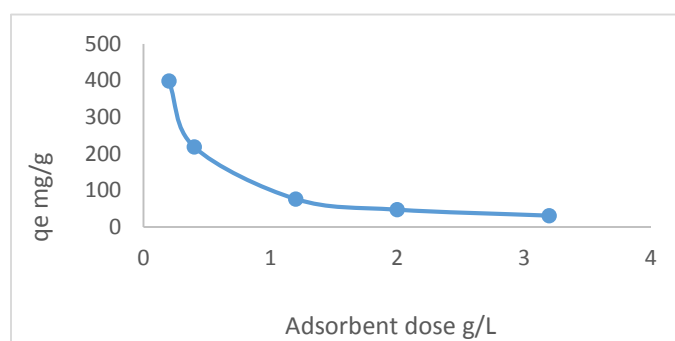


**Fig.11.** Effect of adsorbent (AC/Fe<sub>3</sub>O<sub>4</sub> NPs, 800°C) dosage on the removal of Pb (II), q<sub>e</sub> vs. dose.

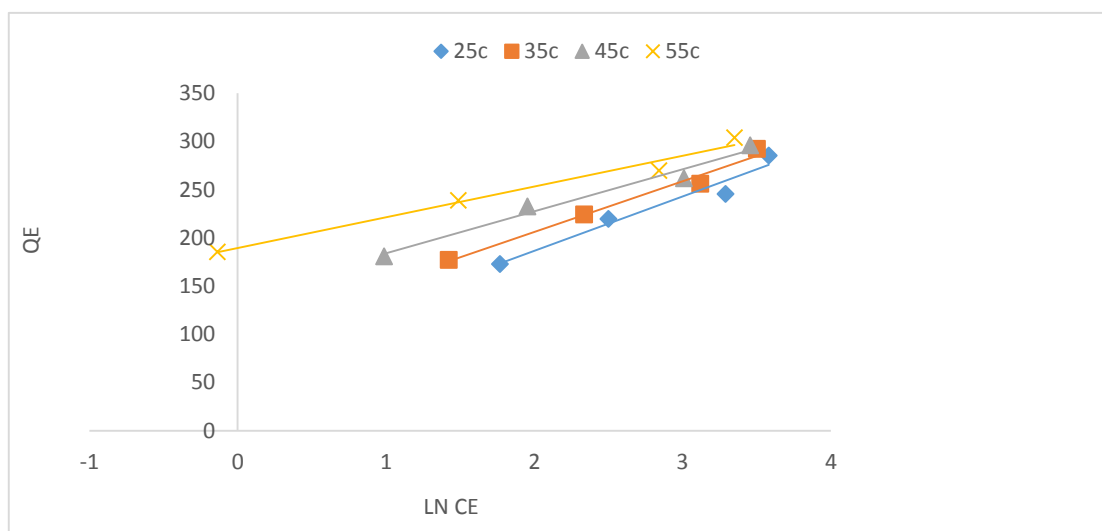
and  $K_L$  (L mg<sup>-1</sup>) is the Langmuir constant related to free energy. Figure 12 shows the Langmuir ( $1/q_e$  vs.  $1/C_e$ ) plots for the adsorption of lead ions at different temperatures. The value of  $Q_m$  and  $k_L$  constants and the correlation coefficients for Langmuir isotherms

are presented in Table 11. The correlation coefficients are between 0.92 and 0.97 suggesting that Langmuir isotherm is less applicable than Tempkin and Freundlich models.

**Freundlich isotherm equation:** This isotherm is

**Table 11.** Adsorption of Pb(II), 100mg/L, onto (AC/Fe<sub>3</sub>O<sub>4</sub> NPs, 800°C), 0.4g/L, at constant temperature (25°C) and varied times, compared with calculated experimental  $q_e$  values using first-order, second-order, and intraparticle diffusion rate constants.

Kinetic model	Parameter	
First- order kinetic model	$q_e$ exp. (mg/g)	229.1
	$k_1$ (min. <sup>-1</sup> )	0.02971
	$q_e$ calc. (mg/g)	38.7972
	$R^2$	0.768
Second- order kinetic model	$k_2$ (g mg <sup>-1</sup> min <sup>-1</sup> )	0.0018485
	$h$ (mg g <sup>-1</sup> min <sup>-1</sup> )	99.9728
	$q_e$ calc.(mg/g)	232.558
	$R^2$	0.9995
Intraparticle diffusion	$K_{diff}$ . (mg g <sup>-1</sup> min <sup>-1/2</sup> )	2.2255
	$B_L$ (mg/g)	202.77
	$R^2$	0.967

**Fig.12.** Langmuir isotherm for the adsorption of Pb(II) onto (AC/Fe<sub>3</sub>O<sub>4</sub> NPs, 800°C) at different temperatures, 0.01g/25 ml, at pH 8, contact time 60 min.

applied to describe a heterogeneous system characterized by a heterogenous factor of  $1/n$ . The formation of a monolayer is not assumed to be a necessary requirement for the reversible adsorption described by this model. The following is an expression of the Freundlich model (Freundlich 1907).

$$\log q_e = \log K_f + \frac{1}{n} \log C_e$$

Where  $K_f$  (mg g<sup>-1</sup>) is the Freundlich constant indicating adsorption capacity,  $n$  (L mg<sup>-1</sup>) is the adsorption intensity that is the measure of the change in the affinity of the adsorbate with the change in adsorption density. The Freundlich constants  $K_f$  and  $n$  were calculated from the slope and intercept of the

plot of  $\log q_e$  versus  $\log C_e$  (Redlich & Peterson 1959). Adsorption of lead ions onto adsorbent is shown by a linear Freundlich isotherm (Fig. 13). Examination of the isotherm constants and correlation coefficients  $R^2$  reported in Table 11 shows that the Freundlich model is more applicable to activated carbon than the Langmuir model. The obtained correlation coefficients for AC/Fe<sub>3</sub>O<sub>4</sub> NPs at 800°C range from 0.98 to 0.96.

**Tempkin isotherm equation:** The isotherm model considered the effect of indirect adsorbent–adsorbate interaction isotherms which explained that the heat of adsorption of all molecules on the adsorbent surface layer would decrease linearly with coverage due to adsorbent-adsorbate interactions (Temkin & Pyzhev

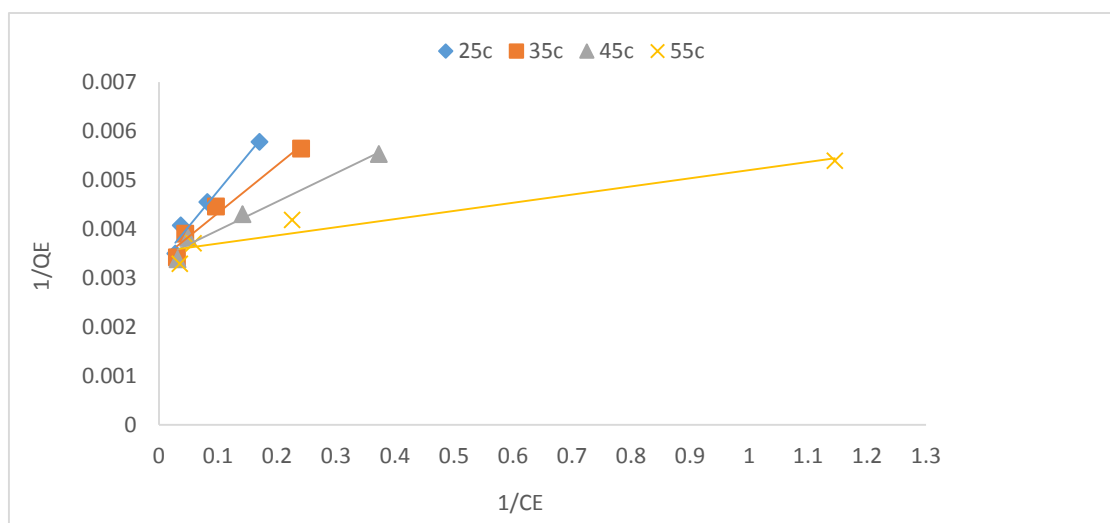


**Fig.13.** Freundlich isotherm for the adsorption of Pb (II) onto (AC/Fe<sub>3</sub>O<sub>4</sub> NPs, at 800°C) at different temperatures, 0.01g/25ml, at pH 8, contact time 60 min.

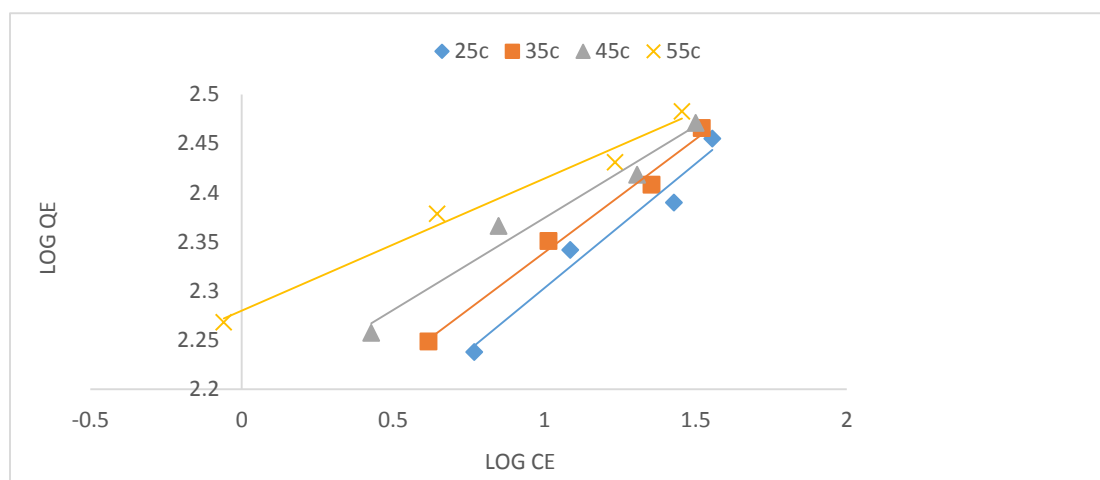


**Fig.14.** Tempkin isotherm for the adsorption of Pb (II) onto (AC/Fe<sub>3</sub>O<sub>4</sub> NPs, 800°C) at different temperatures, 0.01g/25ml, at pH 8, contact time 60 min.

1940; Kavitha & Namasivayam 2007). The linear form of the Tempkin model is as in the equation:

$$q_e = B_T \ln A_T + B_T \ln C_e$$

The adsorption data can be analyzed, according to the equation, from a plot of  $q_e$  versus  $\ln C_e$  Figure 14 at different temperature followed by the determination of the isotherm constants  $A_T$  and  $B_T$  and correlation coefficients (Table 10). The correlation coefficients are between 0.95 and 0.98, suggesting that Tempkin isotherm is less applicable than Freundlich models.

**Adsorption kinetic study:** The kinetic of lead ions adsorption are necessary for determining the optimal

operating conditions for a large-scale batch process. Additionally, it is useful for predicting the adsorption rate (Venn 2008). Thus, the process of lead ions removal from the aqueous phase by the activated carbon (AC/Fe<sub>3</sub>O<sub>4</sub> NPs, 800°C) could be described using pseudo-first order, pseudo-second order, and intraparticle diffusion kinetic models, correlation coefficients were used to express the congruence between experimental data and model-predicted values. The greater the value, the greater its applicability to lead ion adsorption kinetics.

**Pseudo-first order model:** This model assumes that one metal ion is sorbed onto one sorption site on the surface of the adsorbent (Liu et al. 2013). The linear

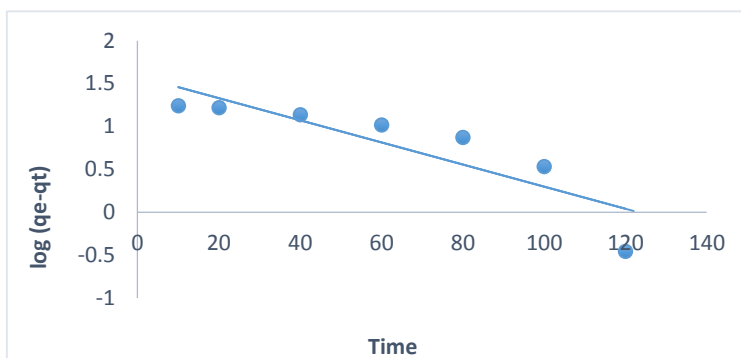


**Fig.15.** Pseudo-first-order kinetics for the adsorption of Pb(II) 100mg/L onto (AC/Fe<sub>3</sub>O<sub>4</sub> NPs, 800°C).

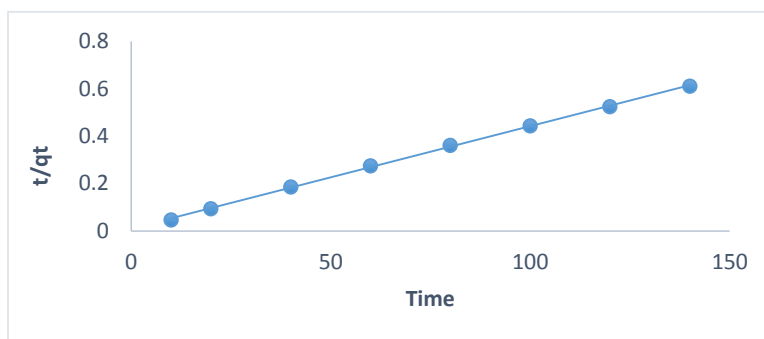


**Fig.16.** Pseudo-second-order kinetics for the adsorption of Pb(II), 100mg/L onto (AC/Fe<sub>3</sub>O<sub>4</sub> NPs, 800°C).

form of the Lagergren model equation:

$$\log(q_e - q_t) = \log q_e - \frac{k_1}{2.303} t$$

Where  $q_e$  and  $q_t$  are the adsorption capacity at equilibrium and at a time  $t$ , respectively ( $\text{mg g}^{-1}$ ) and  $k_1$  is the rate constant ( $\text{min}^{-1}$ ). A plot of  $\log(q_e - q_t)$  versus ( $t$ ) should provide a linear relationship from which  $k_1$  and predicted  $q_e$  can be determined from the slope and intercept of the plot respectively (Fig. 15) i.e. the experimental data do not suit the Lagergren model. In contrast, the calculated  $q_e$  values resulting from linear plots do not match the experimentally obtained  $q_e$  values. This shows that the adsorption of pb(II) on to the activated carbon is not appropriate as the pseudo- first order reaction.

**Pseudo-second-order model:** Ho and McKay's pseudo-second-order kinetics model can be expressed as (Ho & McKay 1999).

$$t / q_t = \frac{1}{k_2 q_e^2} + \frac{1}{q_e} (t)$$

This model assumes that, single metal ion is sorbed onto two sorption sites on the adsorbent's surface. It has been employed to analyze the kinetics of chemisorption from liquid solutions. For the pseudo-second-order model,  $K_2$  ( $\text{g mg}^{-1} \text{min}^{-1}$ ) is the equilibrium rate constant, while  $K_2 q_e$  ( $\text{mg g}^{-1} \text{min}^{-1}$ ) is the initial adsorption rate (Liu et al. 2013). The plot of  $t/q_e$  versus  $t$  shows a linear relationship if the second-order kinetic is applicable. The values of  $k_2$  and  $q_e$  were calculated from the intercept and slope of the linear plots (Fig. 16). The liner plot shows a good agreement between the experimental and calculated  $q_e$  value (Table 12) with a correlation coefficient ( $R^2 = 0.9995$ ), which indicates that the model can be applied for the entire adsorption process and confirms that the adsorption pb(II) on the adsorbent follows the second-order.

**Intraparticle diffusion model:** Adsorption is a multi-step process that involves transporting solute molecules from the aqueous phase to the solid particle surface, where they can then diffuse into the pore interior, it is the rate-determining step and so is

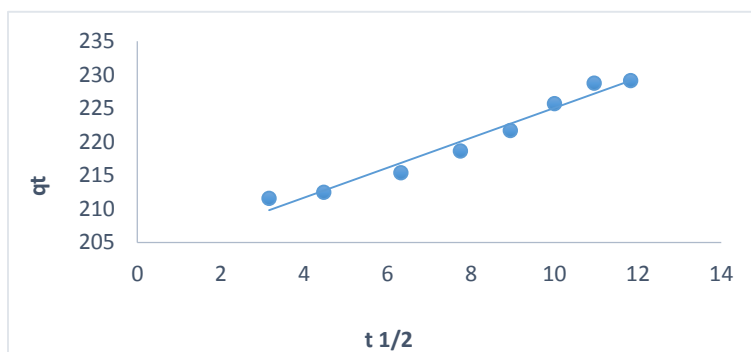


**Fig.17.** Intraparticle diffusion kinetic for the adsorption of Pb(II), 100mg/L onto (AC/Fe<sub>3</sub>O<sub>4</sub> NPs, 800°C).

likely to take a long time. In order to investigate the possibility of the intraparticle diffusion resistance affecting the adsorption intra diffusion model is explored: (El Nemr 2009).

$$q_t = k_{dif} t^{1/2} + B_L$$

Where  $B_L$  is the intercept and  $k_{dif}$  (mg g<sup>-1</sup> min<sup>1/2</sup>) is the intra-particle diffusion rate constant. Figure 17 represents a plot of  $q_t$  versus  $t^{1/2}$  for the adsorbent. Table 11 shows the intercept  $B_L$  and the rate constant  $k_{dif}$ , which can be directly calculated from the slope of the regression line. The  $B_L$  value gives an estimate of the boundary layer thickness. In other words, the bigger the intercept, the bigger the effect of the boundary layer. The linearity of the plots demonstrates that intra-particle diffusion plays a significant role in the uptake of the lead ions by the AC/Fe<sub>3</sub>O<sub>4</sub> NPs, 800°C (Ho, 2003; Crini 2007). The correlation coefficients, obtained were lower compared to those from the pseudo-second-order kinetic model.

## Conclusion

In this study, the synthesized nanocomposite (AC/Fe<sub>3</sub>O<sub>4</sub> at 800°C) was used as an adsorbent to remove Pb(II) from aqueous solutions. The optimum reaction conditions to obtain maximum lead ion uptake were found to be: reaction temperature and time were 55°C, and 140 min., respectively. The absorbent was highly sensitive to pH, with several adsorptions of lead ions observed in pH variations ranging from 3 to 12, and the maximum removal of Pb(II) by 0.4g/L of absorbent was 99.38% at pH 8.

Freundlich's isothermic model fits equilibrium data better than those of Langmuir and Tempkin. Adsorption kinetics following the pseudo-second-order model. TEM analysis revealed that the synthesized nanoparticles have an average particle size of 27nm for Fe<sub>3</sub>O<sub>4</sub> and 17nm for AC/Fe<sub>3</sub>O<sub>4</sub>. The total pore volume of AC/Fe<sub>3</sub>O<sub>4</sub> was 0.2776cm<sup>3</sup>/g, and the average pore diameter was greater than 2nm, indicating that the carbons were highly mesoporous. The BET surface area of AC/Fe<sub>3</sub>O<sub>4</sub> is 397.88 m<sup>2</sup>/g. Based on these findings, AC/Fe<sub>3</sub>O<sub>4</sub> NPs can be utilized efficiently, economically and environmentally friendly for the purification of water from Pb(II) ions.

## Acknowledgments

The authors are grateful to the Department of Chemistry, Duhok University for providing all the facilities for carrying out this work. The authors are not connected to any organization that has an interest in the paper's subject matter financially, either directly or indirectly.

## References

- Adebayo, A.O. 2013. Investigation on *Pleurotus ferulae* potential for the sorption of Pb (II) from aqueous solution. *Bulletin of the Chemical Society of Ethiopia* 27(1): 25-34.
- Aworn, A.; Thiravetyan, P. & Nakbanpote, W. 2008. Preparation and characteristics of agricultural waste activated carbon by physical activation having micro- and mesopores. *Journal of Analytical and Applied Pyrolysis* 82(2): 279-285.

- Bakatula, E.N.; Richard, D.; Neculita, C.M. & Zagury, G.J. 2018. Determination of point of zero charge of natural organic materials. *Environmental Science and Pollution Research* 25: 7823-7833.
- Budinova, T.; Savova, D.; Tsyntsarski, B.; Ania, C.O.; Cabal, B.; Parra, J.B. & Petrov, N. 2009. Biomass waste-derived activated carbon for the removal of arsenic and manganese ions from aqueous solutions. *Applied Surface Science* 255(8): 4650-4657.
- Crini, G.; Peindy, H.N.; Gimbert, F. & Robert, C. 2007. Removal of CI Basic Green 4 (Malachite Green) from aqueous solutions by adsorption using cyclodextrin-based adsorbent: Kinetic and equilibrium studies. *Separation and Purification Technology* 53(1) 97-110.
- Dave, P.N. & Chopda, L.V. 2014. Application of iron oxide nanomaterials for the removal of heavy metals. *Journal of Nanotechnology* 2014.
- Demirbas, A. 2009. Agricultural based activated carbons for the removal of dyes from aqueous solutions: a review. *Journal of Hazardous Materials* 167(1-3): 1-9.
- Deng, H.; Yang, L.; Tao, G. & Dai, J. 2009. Preparation and characterization of activated carbon from cotton stalk by microwave assisted chemical activation-application in methylene blue adsorption from aqueous solution. *Journal of Hazardous Materials* 166(2-3): 1514-1521.
- Dunlop, D.J. & Özdemir, Ö. 2001. *Rock magnetism: fundamentals and frontiers* (No. 3). Cambridge University Press.
- El Nemr, A. 2007. Pomegranate husk as an adsorbent in the removal of toxic chromium from wastewater. *Chemistry and Ecology* 23(5): 409-425.
- El Nemr, A. 2009. Potential of pomegranate husk carbon for Cr (VI) removal from wastewater: Kinetic and isotherm studies. *Journal of Hazardous Materials* 161(1): 132-141.
- El Qada, E.N.; Allen, S.J. & Walker, G.M. 2006. Adsorption of methylene blue onto activated carbon produced from steam activated bituminous coal: a study of equilibrium adsorption isotherm. *Chemical Engineering Journal* 124(1-3): 103-110.
- Ferdous, D.; Dalai, A.K.; Bej, S.K. & Thring, R.W. 2002. Pyrolysis of lignins: experimental and kinetics studies. *Energy & Fuels* 16(6): 1405-1412.
- Freundlich, H. 1907. Über die adsorption in lösungen. *Zeitschrift für physikalische Chemie* 57(1): 385-470.
- Ghasemi, N.; Ghasemi, M.; Moazeni, S.; Ghasemi, P.; Alharbi, N.S.; Gupta, V.K. & Tkachev, A.G. 2018. Zn (II) removal by amino-functionalized magnetic nanoparticles: Kinetics, isotherm, and thermodynamic aspects of adsorption. *Journal of Industrial and Engineering Chemistry* 62: 302-310.
- Girgis, B.S.; Smith, E.; Louis, M.M. & El-Hendawy, A.N.A. 2009. Pilot production of activated carbon from cotton stalks using H<sub>3</sub>PO<sub>4</sub>. *Journal of analytical and applied pyrolysis*, 86(1), 180-184.
- Gong, G.Z.; Qiang, X.; Zheng, Y.F.; Ye, S.F. & Chen, Y.F. 2009. Regulation of pore size distribution in coal-based activated carbon. *New Carbon Materials* 24(2): 141-146.
- Gupta, V.K. & Nayak, A. 2012. Cadmium removal and recovery from aqueous solutions by novel adsorbents prepared from orange peel and Fe<sub>2</sub>O<sub>3</sub> nanoparticles. *Chemical Engineering Journal* 180: 81-90.
- Ho, Y.S. & McKay, G. 1999. Pseudo-second order model for sorption processes. *Process Biochemistry* 34(5): 451-465.
- Ho, Y.S. 2003. Removal of copper ions from aqueous solution by tree fern. *Water Research* 37(10): 2323-2330.
- Humphrey, J.L. & Keller, G.E. 1997. *Separation process technology* (pp. 113-151). New York: McGraw-Hill.
- Ilankoon, N. 2014. Use of iron oxide magnetic nanosorbents for Cr (VI) removal from aqueous solutions: A review. *Journal of Engineering Research and Applications* 4(10): 55-63.
- Imran, M.; Anwar, K.; Akram, M.; Shah, G.M.; Ahmad, I.; Samad Shah, N. & Schotting, R.J. 2019. Biosorption of Pb (II) from contaminated water onto *Moringa oleifera* biomass: kinetics and equilibrium studies. *International Journal of Phytoremediation* 21(8): 777-789.
- Imran, M.; Khan, Z.U.H.; Iqbal, J.; Shah, N.S.; Muzammil, S.; Ali, S. & Rizwan, M. 2020. Potential of siltstone and its composites with biochar and magnetite nanoparticles for the removal of cadmium from contaminated aqueous solutions: batch and column scale studies. *Environmental Pollution* 259: 113938.
- Imran, M.; Khan, Z.U.H.; Iqbal, M.M.; Iqbal, J.; Shah, N.S.; Munawar, S. & Rizwan, M. 2020. Effect of biochar modified with magnetite nanoparticles and

- HNO<sub>3</sub> for efficient removal of Cr (VI) from contaminated water: a batch and column scale study. *Environmental Pollution* 261: 114231.
- Iqbal, J.; Shah, N.S.; Sayed, M.; Imran, M.; Muhammad, N.; Howari, F.M. & Haija, M.A. 2019. Synergistic effects of activated carbon and nano-zerovalent copper on the performance of hydroxyapatite-alginate beads for the removal of As<sup>3+</sup> from aqueous solution. *Journal of Cleaner Production* 235: 875-886.
- Ismadji, S.; Sudaryanto, Y.; Hartono, S.B.; Setiawan, L.E.K. & Ayucitra, A.J.B.T. 2005. Activated carbon from char obtained from vacuum pyrolysis of teak sawdust: pore structure development and characterization. *Bioresource Technology* 96(12): 1364-1369.
- Jain, M.; Yadav, M.; Kohout, T.; Lahtinen, M.; Garg, V.K. & Sillanpää, M. 2018. Development of iron oxide/activated carbon nanoparticle composite for the removal of Cr (VI), Cu (II) and Cd (II) ions from aqueous solution. *Water Resources and Industry* 20: 54-74.
- Juan, Y. & Ke-Qiang, Q. 2009. Preparation of activated carbon by chemical activation under vacuum. *Environmental Science & Technology* 43(9): 3385-3390.
- Karaca, M. 2008. Biosorption of aqueous Pb<sup>2+</sup>, Cd<sup>2+</sup>, and Ni<sup>2+</sup> ions by *Dunaliella salina*, *Oocystis* sp., *Porphyridium cruentum*, and *Scenedesmus protuberans* prior to atomic spectrometric determination (Doctoral dissertation, Izmir Institute of Technology (Turkey)).
- Karagöz, S.; Tay, T.; Ucar, S. & Erdem, M. 2008. Activated carbons from waste biomass by sulfuric acid activation and their use on methylene blue adsorption. *Bioresource Technology* 99(14): 6214-6222.
- Katsaros, F.K.; Steriotis, T.A.; Romanos, G.E.; Konstantakou, M.; Stubos, A.K. & Kanellopoulos, N. K. 2007. Preparation and characterisation of gas selective microporous carbon membranes. *Microporous and Mesoporous Materials* 99(1-2): 181-189.
- Kaur, M.; Kumar, M.; Sachdeva, S. & Puri, S.K. 2018. Aquatic weeds as the next generation feedstock for sustainable bioenergy production. *Bioresource Technology* 251: 390-402.
- Kavitha, D., & Namasivayam, C. (2007). Experimental and kinetic studies on methylene blue adsorption by coir pith carbon. *Bioresource Technology* 98(1): 14-21.
- Li, X.; Qiu, J.; Hu, Y.; Ren, X.; He, L.; Zhao, N. & Zhao, X. 2020. Characterization and comparison of walnut shells-based activated carbons and their adsorptive properties. *Adsorption Science & Technology* 38(9-10): 450-463.
- Lin, S.H. & Juang, R.S. 2009. Adsorption of phenol and its derivatives from water using synthetic resins and low-cost natural adsorbents: a review. *Journal of Environmental Management* 90(3): 1336-1349.
- Liu, Y.; Chen, M. & Yongmei, H. 2013. Study on the adsorption of Cu (II) by EDTA functionalized Fe<sub>3</sub>O<sub>4</sub> magnetic nano-particles. *Chemical Engineering Journal* 218: 46-54.
- Lu, X.; Jiang, J.; Sun, K. & Xie, X. 2014. Preparation and characterization of sisal fiber-based activated carbon by chemical activation with zinc chloride. *Bulletin of the Korean Chemical Society* 35(1): 103-110.
- Malarvizhi, R. & Sulochana, N. 2008. Sorption isotherm and kinetic studies of methylene blue uptake onto activated carbon prepared from wood apple shell. *Journal of Environmental Protection Science* 2: 40-46.
- Malik, P.K. 2003. Use of activated carbons prepared from sawdust and rice-husk for adsorption of acid dyes: a case study of Acid Yellow 36. *Dyes and Pigments* 56(3): 239-249.
- Mall, I.D.; Srivastava, V.C.; Agarwal, N.K. & Mishra, I.M. 2005. Removal of congo red from aqueous solution by bagasse fly ash and activated carbon: kinetic study and equilibrium isotherm analyses. *Chemosphere* 61(4): 492-501.
- Muhamad, S.G.; Esmail, L.S. & Hasan, S.H. 2016. Kinetic studies of bioethanol production from wheat straw. *ZANCO Journal of Pure and Applied Sciences* 28(3): 97-103.
- Ojemaye, M.O.; Okoh, O.O. & Okoh, A.I. 2017. Surface modified magnetic nanoparticles as efficient adsorbents for heavy metal removal from wastewater: Progress and prospects. *Materials Express* 7(6): 439-456.
- Oliveira, L.C.; Goncalves, M.; Oliveira, D.Q.; Guerreiro, M.C.; Guilherme, L.R. & Dallago, R.M. 2007. Solid waste from leather industry as adsorbent of organic dyes in aqueous-medium. *Journal of Hazardous*

- Materials 141(1): 344-347.
- Rampe, M.J.; Santoso, I.R.; Rampe, H.L.; Tiwow, V.A. & Apita, A. 2021. Infrared Spectra Patterns of Coconut Shell Charcoal as Result of Pyrolysis and Acid Activation Origin of Sulawesi, Indonesia. In E3S Web of Conferences (Vol. 328, p. 08008). EDP Sciences.
- Redlich, O.J.D.L. & Peterson, D.L. 1959. A useful adsorption isotherm. *Journal of Physical Chemistry* 63(6): 1024-1024.
- Reffas, A.; Bernardet, V.; David, B.; Reinert, L.; Lehocine, M.B.; Dubois, M. & Duclaux, L. 2010. Carbons prepared from coffee grounds by H<sub>3</sub>PO<sub>4</sub> activation: Characterization and adsorption of methylene blue and Nylosan Red N-2RBL. *Journal of Hazardous Materials* 175(1-3): 779-788.
- Rufford, T.E.; Hulicova-Jurcakova, D.; Zhu, Z. & Lu, G.Q. 2009. Empirical analysis of the contributions of mesopores and micropores to the double-layer capacitance of carbons. *The Journal of Physical Chemistry C* 113(44): 19335-19343.
- Saeed, A.; Akhter, M.W. & Iqbal, M. 2005. Removal and recovery of heavy metals from aqueous solution using papaya wood as a new biosorbent. *Separation and Purification Technology* 45(1): 25-31.
- Saleh, T.A. & Gupta, V.K. 2012. Column with CNT/magnesium oxide composite for lead (II) removal from water. *Environmental Science and Pollution Research* 19: 1224-1228.
- Sanchez, C.; Arribart, H. & Giraud Guille, M.M. 2005. Biomimetism and bioinspiration as tools for the design of innovative materials and systems. *Nature Materials* 4(4): 277-288.
- Sharififard, H.; Nabavinia, M. & Soleimani, M. 2017. Evaluation of adsorption efficiency of activated carbon/chitosan composite for removal of Cr (VI) and Cd (II) from single and bi-solute dilute solution. *Advances in Environmental Technology* 2(4): 215-227.
- Spahis, N.; Addoun, A., Mahmoudi, H. & Ghaffour, N. 2008. Purification of water by activated carbon prepared from olive stones. *Desalination* 222(1-3): 519-527.
- Tahir, B. & Mezori, H.A. 2020. Bioethanol production from *Quercus aegilops* using *Pichia stipitis* and *Kluyveromyces marxianus*. *Biomass Conversion and Biorefinery* 1-10.
- Temkin, M.J. & Pyzhev, V. 1940. Recent modifications to Langmuir isotherms.
- Tran, D.L.; Le, V.H.; Pham, H.L.; Hoang, T.M.N.; Nguyen, T.Q.; Luong, T.T. & Nguyen, X.P. 2010. Biomedical and environmental applications of magnetic nanoparticles. *Advances in Natural Sciences: Nanoscience and Nanotechnology* 1(4): 045013.
- Vazquez, G.; Gonzalez-Alvarez, J.; Freire, S.; López-Lorenzo, M. & Antorrena, G. 2002. Removal of cadmium and mercury ions from aqueous solution by sorption on treated *Pinus pinaster* bark: kinetics and isotherms. *Bioresource Technology* 82(3): 247-251.
- Venn, R.F. 2008. Principles and practice of bioanalysis. CRC Press.
- Wang, G.; Li, W.; Li, B. & Chen, H. 2008. TG study on pyrolysis of biomass and its three components under syngas. *Fuel* 87(4-5): 552-558.
- Wang, S.; Zhu, Z.H.; Coomes, A.; Haghseresht, F. & Lu, G.Q. 2005. The physical and surface chemical characteristics of activated carbons and the adsorption of methylene blue from wastewater. *Journal of Colloid and Interface Science* 284(2): 440-446.
- Wibowo, N.; Setyadi, L.; Wibowo, D.; Setiawan, J. & Ismadji, S. 2007. Adsorption of benzene and toluene from aqueous solutions onto activated carbon and its acid and heat treated forms: influence of surface chemistry on adsorption. *Journal of Hazardous Materials* 146(1-2): 237-242.
- Yao, X.; Xu, K. & Liang, Y. 2016. Comparing the thermo-physical properties of rice husk and rice straw as feedstock for thermochemical conversion and characterization of their waste ashes from combustion. *BioResources* 11(4): 10549-10564.
- Zhang, H.; Li, X.; He, G.; Zhan, J. & Liu, D. 2013. Preparation of magnetic composite hollow microsphere and its adsorption capacity for basic dyes. *Industrial & Engineering Chemistry Research* 52(47): 16902-16910.